

# Ductile cast iron inserts for spent nuclear fuel disposal: radiography and fractography

F. Lofaj<sup>1,2\*</sup>, L. Metten<sup>1</sup>, A. van de Sande<sup>1</sup>, K.-F. Nilsson<sup>1</sup>, A. Eriksson<sup>1</sup>

<sup>1</sup>Joint Research Centre – EC, Institute for Energy, P.O. Box 2, 1755 ZG Petten, The Netherlands

<sup>2</sup>Institute of Materials Research of the Slovak Academy of Sciences, Watsonova 47, 043 53 Košice, Slovak Republic

Received 2 June 2006, received in revised form 15 November 2006, accepted 1 December 2006

## Abstract

The paper presents an exploratory study for non-destructive techniques that can be used to detect and characterize the defects in large ductile cast iron (DCI) containers for geological disposal of spent nuclear fuel. Non-destructive examination of the defects in DCI inserts is necessary to meet its acceptance criteria. The aim of the work was to investigate the ability of film radiography in detection of microstructure defects in DCI inserts in the as-produced state as well as heavily deformed components and subsequent identification of the indications via conventional destructive techniques. Radiography of outer insert walls in the as-produced inserts combined with metallography detected slag inclusions at the inner surfaces of the channels. Numerous cracks were detected in the deformed canister walls. Cracks were initiated at large slag defects in the zone of tensile stresses and ductile tearing was identified as a mechanism of their growth.

**Key words:** spent nuclear fuel, geological disposal, ductile cast iron, non-destructive testing, radiography

## 1. Introduction

A significant revival of the interest to nuclear energy in the last years occurred due to the increased energy prices and because it is seen as a key component in an energy mix to mitigate global warming [1]. Solutions for the safe and long-term management of spent nuclear fuel and high-level radioactive waste are necessary if nuclear energy shall constitute an important part of the energy mix. Presently there are no methods for total elimination of the toxicity of radioactive waste but geological disposal is seen as the most feasible long-term solution. A geological disposal system is based on a multi-barrier system with engineered barriers as well as geological barriers that isolate the waste and retard the migration of radionuclides. The actual system depends on the geological formation (clay, crystalline rock or tuff) but the overall safety should be comparable. In the Scandinavian system, crystalline rock is used for direct disposal of spent nuclear fuel with a copper/cast iron canister (Fig. 1) at a depth of 500–700 m surrounded by a bentonite buffer as the engineered barriers [2]. Crystalline rock



Fig. 1. Full size model of the KBS-3 canister for geological disposal of the spent nuclear fuel.

is very stable and though it may contain fractures, together with bentonite act as secondary barrier. The canister is seen as the primary barrier, which has to

\*Corresponding author: <sup>1</sup>tel.: +31 22 456 5308; fax: +31 22 456 5641; e-mail address: [frantisek.lofaj@jrc.nl](mailto:frantisek.lofaj@jrc.nl)

<sup>2</sup>tel.: +421 557922464; fax: +421 557922408; e-mail address: [flofaj@imr.saske.sk](mailto:flofaj@imr.saske.sk)

provide leak-tight containment of radionuclides. The time until the spent nuclear fuel has the same radio-toxicity as the natural uranium is  $10^5$ – $10^6$  years. This gives an indication of the canister design life. Disposal of spent fuel from 12 reactors in Sweden after 40 operational years will require about 4500 canisters. All of them have to be totally leak-tight during the design life. In time spans of several hundred thousands of years, Scandinavia may undergo several ice-ages with ice-sheets up to 3 km thick. Their load will generate stress of 30 MPa and after adding the stress from the swelling of bentonite, a maximum isostatic pressure of about 44 MPa on the canisters was obtained [3]. Shear movements that may follow an ice-age is another severe load case that the canisters need to sustain. A critical issue is to guarantee that manufactured canisters do not have defects that may cause loss of integrity even under these extreme conditions. A three-year program was performed by Svensk Kärnbränslehantering AB (SKB), other Scandinavian partners and JRC to determine failure probabilities for manufactured KBS-3 canisters and the associated acceptance criteria for defects and material data [3] for the hydrostatic ice-age load case.

Reproducible fabrication technology and reliable non-destructive examination (NDE) of each copper shielding and the ductile cast iron (DCI) insert are necessary to guarantee that acceptance criteria are fulfilled. NDE studies at SKB have focused on the copper shielding whereas JRC investigated cast iron inserts. Earlier microstructure and tensile test studies revealed that DCI inserts contain a variety of technological defects that inferred relatively low values and large scatter of ductility [5, 6]. Typical defects that can affect strength and ductility include [4–7]:

- nodularity of the graphite particles,
- areas with clustered graphite and/or with depleted graphite,
- areas with clustered pores,
- pearlite content,
- large inclusions or areas of secondary phases with Mg-, Si- and Fe-oxides, often called slag or dross.

Tensile tests in combination with fractography of the samples taken from DCI inserts pointed to large slag defects in the form of oxidation films as the main cause for low ductility. However, other microstructure properties such as low nodularity and high pearlite content may also reduce ductility [4–6]. Obviously, casting procedures that minimize the number and size of slag defects in combination with reliable NDE techniques are essential to guarantee the long-term functioning of the canisters. At the same time, stress distribution occurs in the canister wall under global compression. Finite element modeling showed that tensile stresses develop in DCI insert walls at the interface with steel tubes under large compressive loads [3, 8]. Defects in such a region would be more critical than

in regions with compressive stresses and the emphasis for the NDE inspection for defects should be there.

The most practical and economical methods for NDE of canisters on an industrial basis are ultrasonic and radiography methods. Obviously, each technique has some advantages and limitations, especially in the case of complex geometry of the inserts. The aim of the current work is to investigate the potential of radiography techniques for the detection of technological and other operational defects in ductile cast iron inserts, to characterize the defects detected by radiography, to assess suitability of this technique in the development of acceptance criteria for DCI inserts in nuclear waste canisters and to contribute to the development of inspection and qualification methods for waste packages. The NDE analyses are performed on the canister I26 from the research program [3] and include insert segments in “as-received insert” as well as segments from one mock-up that had been heavily deformed during a large isostatic pressure tests [10, 11], referred “as-deformed insert”.

## 2. Experimental procedure

### 2.1. Material characterization

The subject of the study included one insert designated as I26. It was cast using a top pouring technique. The material for the inserts is ductile cast iron grade EN-GJS-400-15U (European standard EN 1563) [9]. Together with high strength properties and improved ductility, this material possesses good castability. The chemical compositions of the material from this insert are given in Table 1 [5].

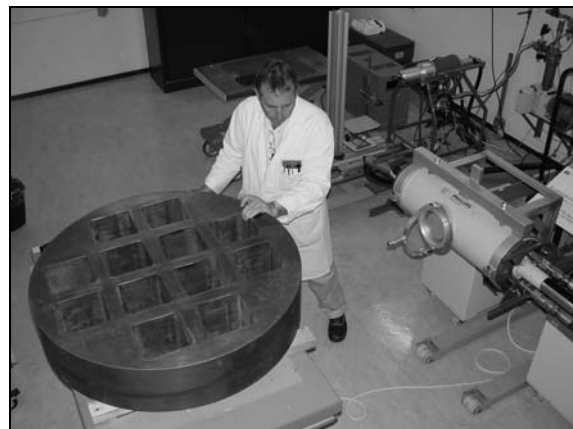


Fig. 2. Around 200 mm thick slab cut from the insert I26 and the setup for the radiographic inspection with the industrial 450 kV X-ray source. The sections that were cut from similar slabs for radiographic and microstructure investigations are indicated.

Table 1. Chemical analysis of ductile cast iron in the I26 insert [5]

Insert composition	C (wt.%)	Si (wt.%)	Mn (wt.%)	P (wt.%)	S (wt.%)	Cr (wt.%)	Ni (wt.%)	Mo (wt.%)	Cu (wt.%)	Mg (wt.%)
I26	3.56	2.39	0.52	0.03	0.01	–	0.73	–	–	0.06

*Sample selection:* Because of handling difficulties, 5 m long I26 insert was cut into several pieces with different lengths. Two full cross-sections with the length of 50 mm and 200 mm (Fig. 2) and several smaller segments obtained from another cross-section were used in the current study.

Another 700 mm segment of I26 insert was used to produce the canister mock-up for pressure test. It was placed in the sealed copper over-pack. The differences compared to real canister were the reduced length to fit into a pressure vessel and the absence of spent fuel in the channels. The total length and weight of the mock-up were 1050 mm and 5 tons, respectively. The mock-up was subjected to the hydrostatic compressive stress up to 130 MPa for 120 s in a cold isostatic press (model ASEA Quintus) at Schunk Kohlenstofftechnik in Heuchelheim, Germany [10, 11]. The deformation of the canister was measured after test and the insert was extracted from the overpack. Then, four segments with the length of 300 mm, 40 mm, 40 mm and 315 mm, respectively, were cut from it for further investigations. The 300 mm cross-section was divided into 5 smaller pieces which were radiographed as a whole. Then, those with cracks were cut into smaller segments for detailed studies.

## 2.2. Film radiography

Radiographic inspection technique consisted of the two different X-ray sources:

- PHILIPS MCN 451 covering the range of energies up to 450 kV. The distance between the source and the film in setup was 0.9 m (Fig. 2).

- Varian Linear Accelerator M3 with energies of 1 MeV and 3 MeV. The distance between the source and the film in this case was 1.5–2 m. The received dose in this inspection was 1.5 Gray. Radiographic films used were Agfa Structurix D2, D4, and D7, with the size of 150 mm × 240 mm. Optical (or photographic) density of the images on the film considered acceptable for valid inspection was in the range 2.3–3.5 D (D is the dimensionless unit of optical density defined as a base 10 logarithm of the ratio of light incident and transmitted through the film). Radiographic images usually exhibit very low contrast and have to be examined in a dark room under strong light source. Printing radiographic images with clearly visible defects required digitization of the image and strong digital enhancement

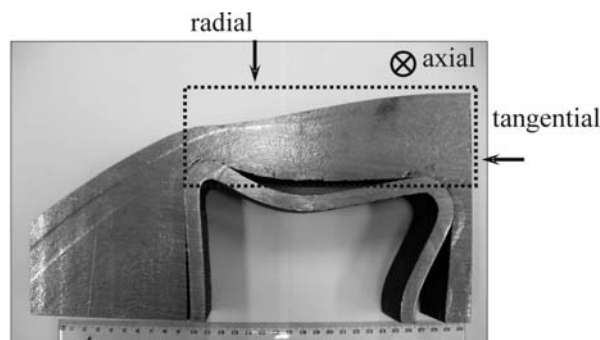


Fig. 3. A 50 mm thick part (designated L1) cut from 300 mm thick cross-section of the deformed mock-up with cracks, which was used for radiographic and microstructure studies. The directions of radiographic examination are indicated. The dotted box indicates the area shown in Fig. 8.

of the contrast and brightness. Such procedure was applied to all radiographic images in the current work.

Radiographic sensitivity and flaw detectability were determined using two different image quality indicator (IQI) standard steel reference blocks with artificial defects and size 80 mm (w) × 120 mm (l) × 85 mm (t). The first IQI reference block (RB 1) contained four sets of six 100 μm wide grooves with the depths of 15 mm, 10 mm, 5 mm, 2.5 mm, 1.25 mm and 0.6 mm. The second IQI reference block (RB 2) contained a set of thirteen pairs of grooves and holes. The groove widths and hole diameters were equal to their depth and they were 1.6 mm, 1.28 mm, 1.045 mm, 0.83 mm, 0.665 mm, 0.50 mm, 0.42 mm, 0.365 mm, 0.285 mm, 0.22 mm, 0.20 mm, 0.125 mm, and 0.12 mm, respectively.

The sensitivity was determined using two types of IQI wire penetrameters depending on the thickness of the tested material. The penetrometer 1 FE DIN with the set of 7 wires with diameters from 3.20 mm (wire No. 1) to 0.80 mm (No. 7) was used for the materials 40–160 mm thick. The penetrometer 6 FE DIN with the wires No. 6–12 having diameters from 1.00 mm up to 0.25 mm was used for the blocks with the thickness in the range from 12.5 mm to 50 mm.

The two hundred millimeter thick insert slab (see Fig. 2) and the segments (Fig. 3) cut from 300 mm and 315 mm long mock-up cross-sections were examined in radial and axial directions to visualize possible defects

in the insert walls between the square steel tube channels and curved surface of the insert.

**Metallography:** Defect identification and microstructure characterization were performed on metallographic sections using light and scanning electron microscopy (SEM). Approximately 1 cm thick slices from the samples from as-produced material were ground and polished using standard procedure involving set of SiC papers and 16  $\mu\text{m}$ , 9  $\mu\text{m}$ , 3  $\mu\text{m}$  and 1  $\mu\text{m}$  diamond suspensions. Their microstructure was revealed by etching in 5% Nital (5%  $\text{HNO}_3$  solution in ethanol) for 15–20 s. Image analysis and the measurements of nodule size and shape distributions were performed automatically with dedicated software on approximately  $\sim 1400$  nodules in both axial and radial directions. Crack morphology and possible crack growth mechanisms in the mock-up samples were studied on the polished side surfaces using SEM.

### 3. Results

#### 3.1. Film radiography

**IQI reference blocks:** Visibility and detectability tests in RB1 and RB2 blocks performed with the high resolution film Agfa Structurix D2 revealed that 100  $\mu\text{m}$  wide grooves, which are  $\geq 1.25$  mm deep and volumetric indications (holes) with the size  $\geq 0.4$  mm can be detected (Fig. 4a). In the case of the medium resolution Agfa Structurix D4 film, 100  $\mu\text{m}$  grooves with the depth  $\geq 2.5$  mm and volumetric defects with the size  $\geq 0.67$  mm were detectable (Fig. 4b). Maximum detectability of the low resolution film Agfa Curix blue HC-S Plus was  $\geq 5$  mm for 100  $\mu\text{m}$  grooves and  $\geq 0.8$  mm for volumetric defects (Fig. 4c).

**As-produced insert:** Both slices from I26 insert, 50 mm and 200 mm thick were examined in axial direction. The results from a 50 mm slice are shown in Fig. 5 and Fig. 6. The largest defects include casting blowholes and/or their clusters adjacent to the steel channel bridging strips and debonding between the matrix and steel channels (see arrows in Fig. 5). The size of blowhole indicated between the channels is almost 17 mm. It seems to be one hole rather than agglomerate of several holes formed near the insert during casting. Debonding between the matrix and steel tubes is relatively often visible around the corners of the channels. Figure 6a shows several dark indications scattered in the bulk and individual indications and their agglomerates near the channel surfaces. Note the indications from 6 FE DIN IQI wire penetrameter in the center of this figure. The thinnest wire visible on the film was the wire No. 10 with the diameter of 0.40 mm. Thus, the radiographic sensitivity in this case corresponds to 0.8 %, which is considerably better than 2 % limit used in industry.

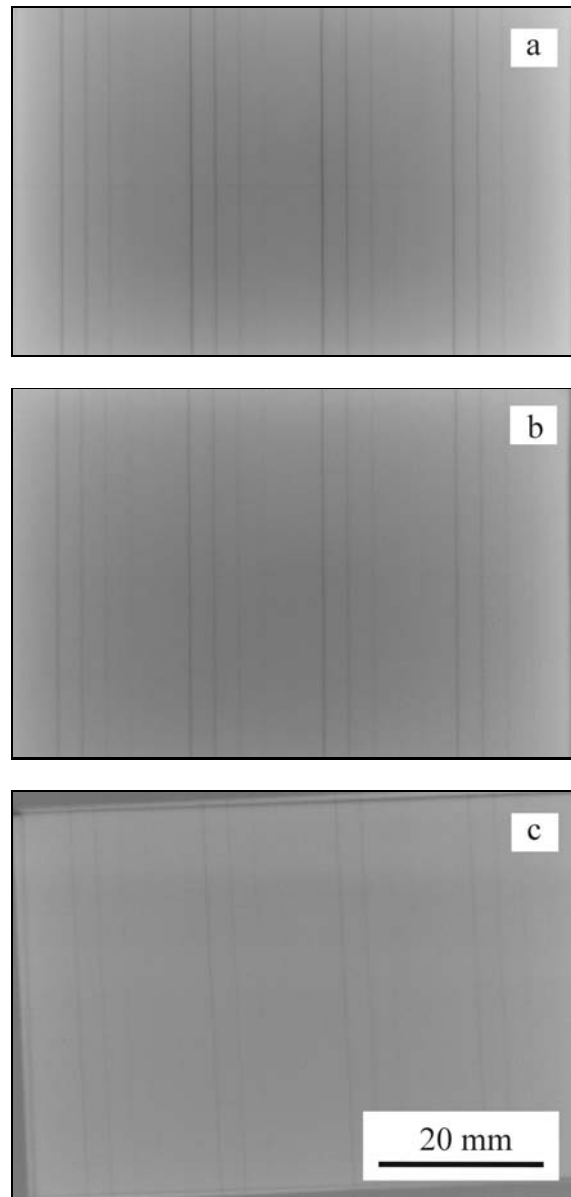


Fig. 4. The comparison of detectability and visibility of the artificial cracks in IQI reference block RB1 using: a) high resolution Agfa Structurix D2 film; b) medium resolution Agfa Structurix D4 film; and c) low resolution film Agfa Curix blue HC-S Plus film.

Figure 6b shows similar indications along channel surface at the interface with steel tube. The examination of 200 mm thick slice revealed principally the same defects – blowholes, debonding and inclusions, however, the contrast was considerably lower. The largest blowholes observed were around 10 mm in diameter.

The same measurements were performed with 3 MeV accelerating voltage. The radiographic sensitivity for the 50 mm thick segment was 0.6 % and 320  $\mu\text{m}$  indications were visible. In the case of 200 mm

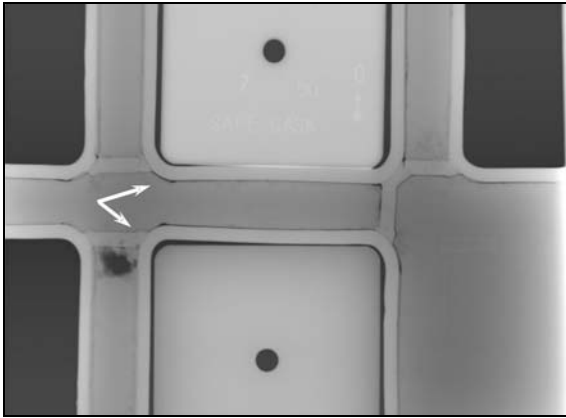


Fig. 5. Large blowholes adjacent to the bridging strip fixing neighboring steel and partial debonding between the tubes and cast iron (see arrows) are visible in 50 mm slice of I26 insert examined in axial direction.

thick slice sensitivity was 0.5 % and the indications of around 1000  $\mu\text{m}$  were visible.

*Deformed insert:* Radiographic testing of 300 mm thick mock-up segments was focused on the changes in the microstructure, which may result from pressure test. Firstly, five insert walls were examined at 3 MeV in radial direction. The source was 2 m away of the outer surface and radiographic film was placed at the inner surface of the steel tubes. The projection of the canister wall in segment L1 is shown in Fig. 7. Note that the exposure conditions at the left and right side of the image vary due to the wall thickness change. Because of limited dynamic range of the film, the optical density acceptable for valid examination is in the zone of less than 1/3 of the wall. The remaining areas of canister wall are either over- or under-exposed and

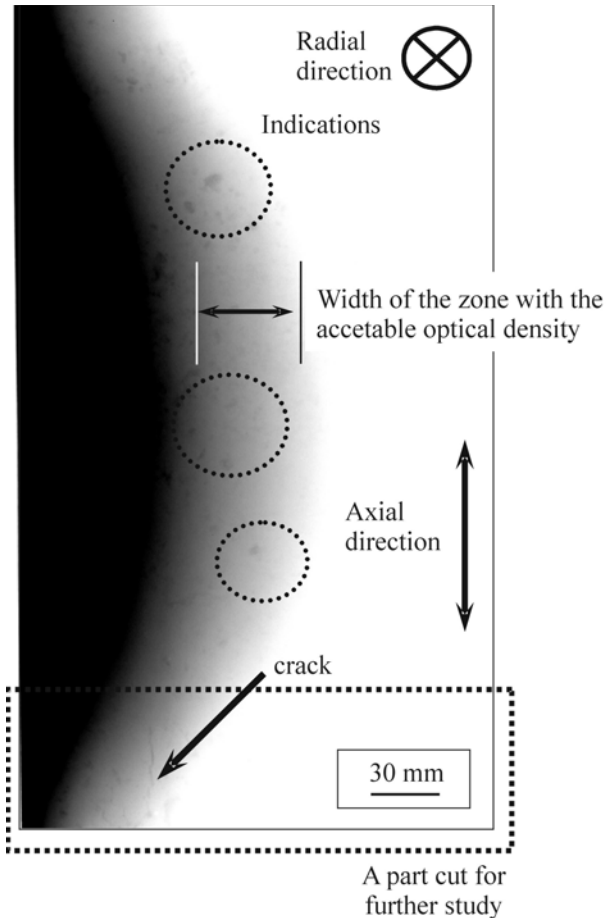


Fig. 7. Radiographic image of the side wall of L1 segment from the mock-up with large cracks in radial direction. The zone with the largest crack in the dotted box was cut for further studies (see Figs. 8 and 9). The variation in wall thickness causes that only a narrow zone in the radiograph exhibits optical density of 2.3–3.5 D, which is suitable for the inspection.

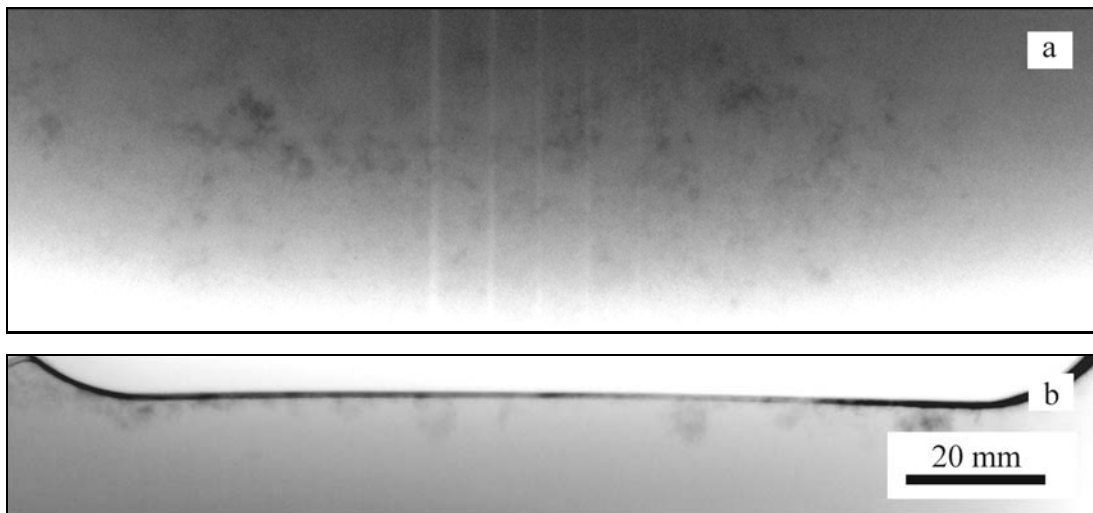


Fig. 6. a) The indications (dark spots) in the bulk of the cast iron; the wire penetrameter was put on the sample; b) the inclusions along the interface with the steel tube.

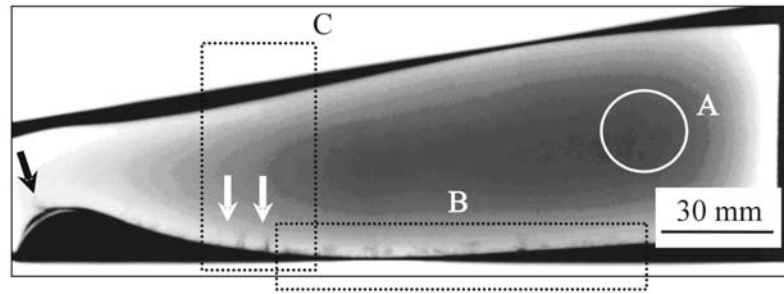


Fig. 8. Radiographic image of the area indicated in Fig. 3 in axial direction revealed clusters of inclusions (A), multiple inclusions along the inner surface (box B), large cracks at the inner surface (box C with two arrows) and additional cracks at the channel corner (arrow). The zone C corresponds to the zone with the cracks in Fig. 7.

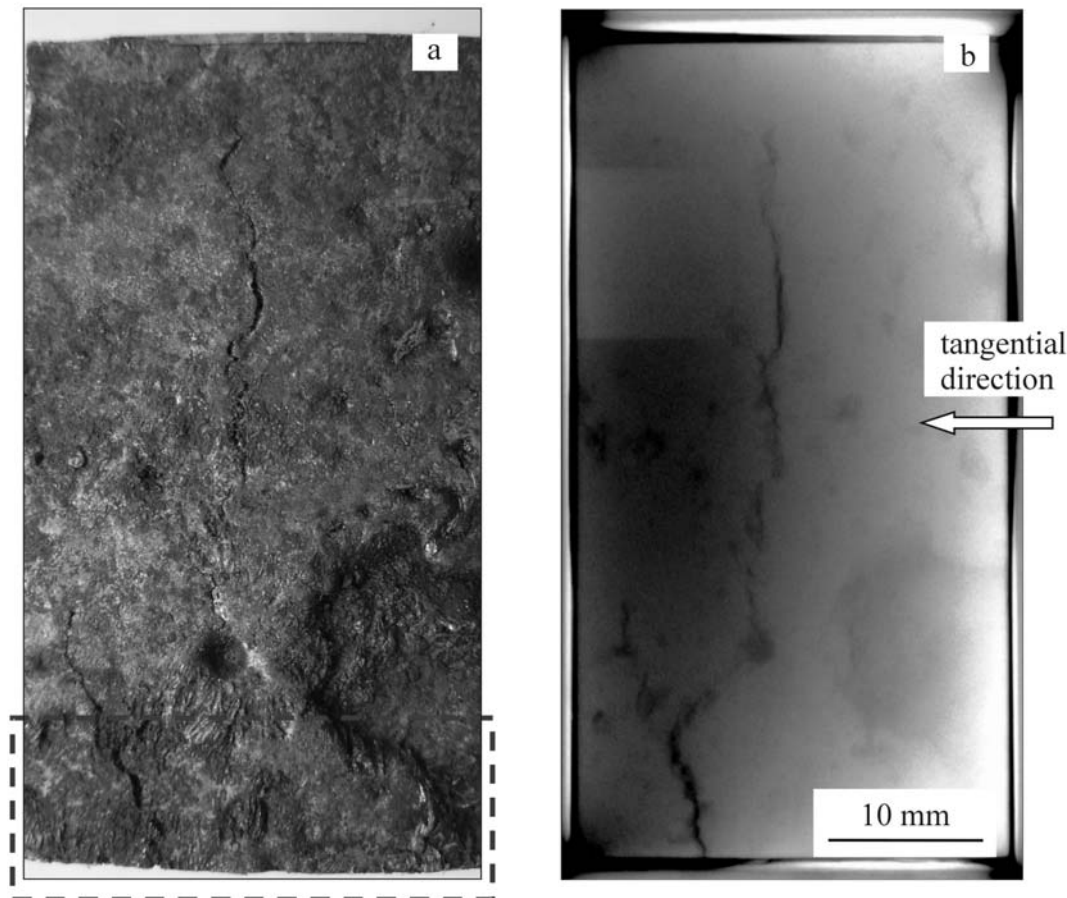


Fig. 9. a) Optical macrograph of the channel wall surface zone with two cracks from Fig. 8 after cutting. The box indicates a sample cut for subsequent fractography study; b) detail of radiographic image of this zone.

additional experiments with optimized exposure are required for full inspection of the wall. The indications similar to those in the as-produced material are marked by circles, and several radial, surface breaking cracks are shown by an arrow in Fig. 7. These cracks were up to 40 mm long. Two other segments contained four cracks from 18 mm up to 38 mm and three cracks from 4 mm up to 17 mm, respectively. The remaining two segments contained only inclusions with a large amount of surface defects.

The segment L1 with the largest cracks was chosen for further study. An approximately 50 mm thick part with cracks (the box in Fig. 7) was cut from L1. The obtained segment is shown in Fig. 3 and the zone of outside wall in the box was studied in axial direction. Both top and bottom sides of this slice were subsequently ground to prevent overlapping of surface roughness with the internal defects. Figure 8 shows radiographic image of this piece in axial direction. Optical density of the films is approxim-

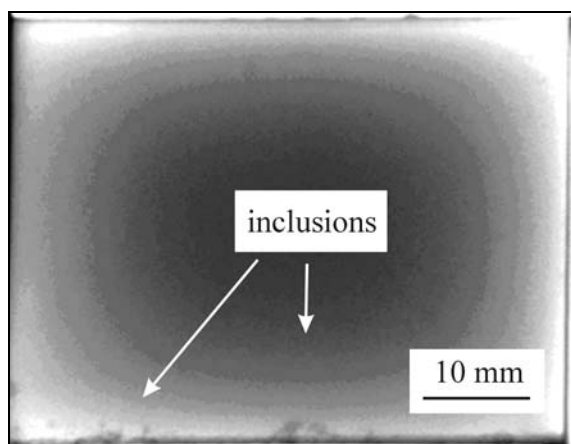


Fig. 10. Radiographic image of the segment from Fig. 9a in tangential direction.

ately constant due to constant thickness of the slice. At least two cracks near the inner surface of the insert wall (see two arrows) were found besides relatively large indications in the bulk of the wall (A), numerous smaller indications under the inner surface (box B) and another crack in the corner of the channel (see arrow). Cracks in the insert wall seem to result from the pressure test, because they were never observed in the walls of the as-produced inserts.

The zone with two cracks in box B was cut out of the insert wall and the cut surfaces were ground parallel. Optical macrograph of inner surface of the insert wall with the cracks is in Fig. 9a and the corresponding radiographic image is in Fig. 9b. The cracks in Fig. 9a appear to be separated but the radiographic image indicates that they are interconnected. They are oriented perpendicular to the surface and generally run along the insert channel despite some crack branching is possible in radial direction. Thus, these cracks are detectable in radial and axial directions. However, they are not visible in tangential direction even on relatively thin slice (see Fig. 10). Only the indications of large inclusions close to the inner surface of the channel are visible.

Radiography is principally unable to detect narrow cracks oriented perpendicularly to the beam. Moreover, even the interpretation of the inclusions and clusters of inclusions is not without problems. The comparison of the surface image and radiographic image in Fig. 9a and 9b indicates that the surface roughness and large surface defects overlap with the indications from the bulk and it is difficult to separate these two groups.

### 3.2. Destructive examination

The purpose of the subsequent destructive examin-

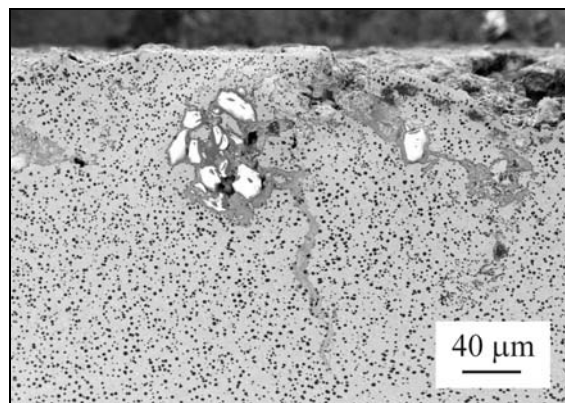


Fig. 11. The most common defects observed in the studied DCI were large inclusions and agglomerates near the surfaces of the insert channels. The other defects accompanying these agglomerates were oxidized zone, holes, cracks and surface roughness.

ation was to identify the indications revealed by radiography. The samples for such study were cut from one of the segments from as-produced sections and from two smaller mock-up parts.

*As-produced material:* The microstructure of the studied material is composed mostly of ferrite matrix. Ferrite grain size varies from less than  $10\ \mu\text{m}$  up to more than  $100\ \mu\text{m}$  with the peak in the range from  $50\ \mu\text{m}$  to  $60\ \mu\text{m}$ . Abnormal grains were not observed. Besides ferrite, pearlite phase was also present. Its content was roughly estimated to be up to 10% [7]. Carbon nodules are distributed relatively homogeneously though areas with higher density and nodule size are possible. Typical size of the nodules was in the range from  $20$  to  $70\ \mu\text{m}$ , their shape was mostly close to ideal sphere. Occasionally, nodule agglomerates were present in the matrix.

The largest and possibly the most typical casting defects in the studied material were large inclusions and their agglomerates (Fig. 11). They can easily be seen by a naked eye on the polished/etched surfaces. They are randomly distributed in material volume but their concentration significantly increases at the interfaces with the steel tubes. The size of the individual inclusions varies within wide range  $200\text{--}500\ \mu\text{m} \times 400\text{--}800\ \mu\text{m}$  but smaller and greater inclusions were also present. Their shapes vary from relatively regular, e.g. rectangular and/or hexagonal, up to highly irregular ones. The agglomerate size and shape depend on the number and arrangement of individual particles.

The inclusions are often surrounded by the affected zone and accompanied by crack-like features and holes. The inclusions are non-conductive non-metallic particles. Their EDX analysis and mapping revealed high concentrations of Mg, Si and O, whereas Fe was practically absent. The concentrations of Mg and Si in the surrounding affected areas were reduced compared to the particles themselves. Oxygen content

Table 2. Summary of the microstructure characterization of I26 insert

	Parameter or defect type	Remark	Importance for failure initiation
C nodules	Carbon nodule distribution	relatively homogeneous	small variations observed are not important
	C nodularity	0.85–0.90	small in this nodularity range
	Mean nodule size	~ 20 $\mu\text{m}$ but 80–100 $\mu\text{m}$ nodules are possible	small unless very large C clusters occur
Matrix	Mean ferrite size	~ 50–60 $\mu\text{m}$	small compared to the other defects
	Pearlite content	present; estimated up to 10 %	minor, only if preferred crack formation occurs
Defects	Non-metallic inclusions	present as individual and agglomerates of particles; found especially near channel/tube interface	dangerous in tensile stress zone when large
	Oxide filled cracks	yes; up to several mm	highly dangerous – cracks may be very large
	Blownholes	yes	big holes in tensile stress zone may act as crack initiation centers
	Pinholes	yes	often related to pearlite; not important
	Microcracks	yes	may form crack in the case of large arrays in tensile stress zone
	Surface defects	scabs, wrinkled areas, seams, grooves, sinking marks	if deep, may act as crack initiation centers

remained relatively high and Fe concentration significantly increased. Thus, the inclusions are Mg-silicate slag or dross particles and the surrounding zone is partially oxidized iron matrix. Because the inclusions were mostly found at the inner surfaces of the insert channels, they most probably originate from the sand used to fill steel tubes during casting.

The holes among the inclusions often exhibit sharp edges. This fact together with the specific chemical composition exclude a possibility of blownholes filled with the water corrosion products during sample preparation. However, the rounded holes may be indigenous and result from local misruns due to incomplete casting in between neighboring inclusion grains. Figure 11 also shows large crack-like defects at the inclusion agglomerate. Such cracks may exist as isolated cracks or interconnected to form larger cracks even in the as-produced material. Their length may exceed 1.5 mm and their morphology is similar to that of intergranular brittle fracture without signs of plastic tearing. Besides large blownholes indicated by radiography in Fig. 5, a number of small pinholes and microcracks were found by SEM at large magnifications. Surface defects on the inner wall surfaces seen after removing steel tube included various scabs, wrinkled areas,

seams, grooves and sinking marks. Table 2 summarizes various microstructure parameters and defects found in I26 insert [7].

*Deformed mock-up:* The defects in the mock-up microstructure were identical to those in the as-produced material except cracks found in selected zone of the insert walls. The morphology of such cracks was investigated on side surface of the sample cut as indicated in Fig. 9a. Figure 12 is a small magnification micrograph of one of the cracks, which is around 10 mm long. This agrees well with the size indicated by other means. The fracture surfaces were corroded and it is difficult to exclude at least partial contribution of sample preparation procedure to this corrosion process. Large slag inclusion is directly connected with this crack but it does not seem to be the crack origin. Most probably, true fracture origin was another defect along the crack surface in either direction from the current section.

Figure 13 provides the information about the growth mechanism of such cracks. Distinctively different profiles of the crack lines on both sides of the crack with characteristic internal necking of the matrix ligaments indicate that the crack grew via gradual deformation and tearing of matrix necks among the nodules.

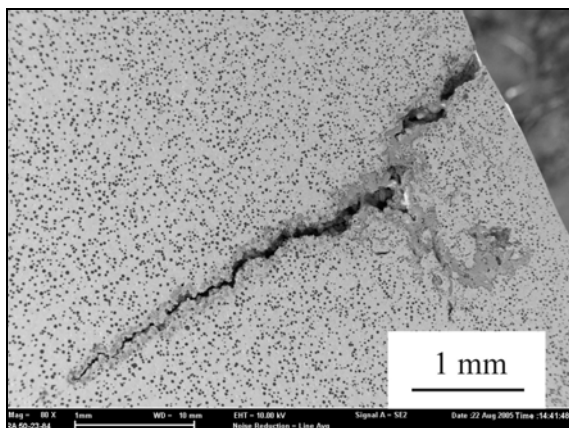


Fig. 12. A profile of the surface breaking crack in L1 mock-up wall (see Fig. 9).

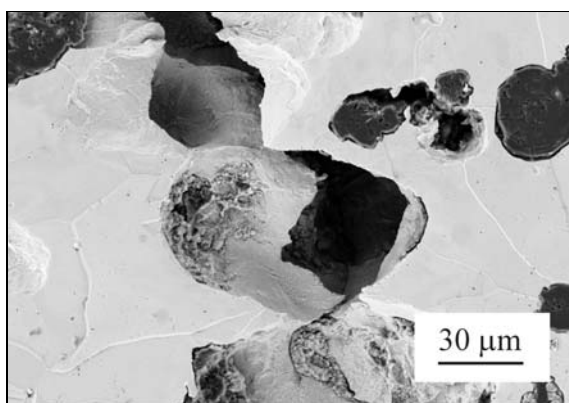


Fig. 13. Crack profile corresponds to typical ductile fracture morphology with intensive internal necking in the ligaments of the matrix among carbon nodules.

#### 4. Discussion

The tests of visibility and detectability showed relatively good possibilities of film radiography in detecting defects. Around 1.25 mm deep cracks and 0.4 mm volumetric defects can be detected using D2 film. Lower resolution film D4 enables detection of 2.5 mm cracks and 0.7 mm holes. These values are considerably smaller than roughly 4–5 mm cracks, which may become critical under stresses exceeding 3 times the maximum calculated compressive stresses in the repository. Thus, radiography is suitable for non-destructive evaluation of the as-received inserts from the viewpoint of resolution.

Preliminary finite element analysis of the stress and strain distributions in the canister subjected to hydrostatic compressive stresses revealed the development of high tensile stresses localized at the inner surface and in the thinnest part of the wall around

channel corner [8]. Apparently, these are the critical locations where cracks preferentially form if suitable initiation centers are present. From this viewpoint, the size of the defects in the zones with the maximum stresses is the critical parameter. Table 2 summarizes also the importance of various defects in DCI insert based on their size. Carbon nodules do not seem to have significant importance at this nodularity range. Although higher number of pinholes and microcracks were localized in pearlite compared to relatively homogeneous ferrite matrix, they may be important only in the case of significant coalescence of such defects. This was not observed yet. The largest in size and often located in the zone with high tensile stresses were slag inclusions and the accompanying oxide-filled cracks. The size of the slag inclusions was up to 1 mm, the oxide-filled cracks can have several millimeters. Thus, they are among the most critical defects, which have to be monitored to prevent insert failure. Deep surface defects such as pits and sinking marks may act as another important failure centers. The cracks were often associated with such surface defects but it is not quite clear if they were initiated from surface defects or from some subsurface defects. Thus, radiography has to be able to visualize large slag inclusions and oxide-filled cracks to fulfill acceptance criteria.

Radiography investigations of the as-produced and deformed materials revealed various indications. The identification of large blownholes and cracks with appropriate orientation was straightforward in both cases. However, optical contrast was insufficient for the detection of crack oriented perpendicularly to the beam. Additional radiographic examination in suitable directions and/or other methods is necessary to visualize cracks with all possible orientations. The remaining indications found in the bulk and near the inner surfaces of the channels correspond very well to the agglomerates of slag inclusions. The identification of small pinholes and small individual inclusions is difficult because of their small size. Moreover, surface defects at the inner insert walls overlap with the volumetric indications when image is acquired in radial direction. It was estimated that in the case of thin samples, a vast majority of the indications may result from surface roughness. The contribution of surface defects would be significantly reduced in relatively thick canister walls. On the other side, sand particles often attached to the inner surfaces of steel tubes would add to the overall image.

Despite difficult identification in these cases, large slag inclusions and cracks with suitable orientation can be visualized and detected. Thus, radiography is able to detect critical defects present in the as-produced inserts and detect cracks with suitable orientation but additional examination is required to visualize cracks oriented perpendicular to the beam.

Besides detectability, time period necessary for ra-

diographic inspection of the corresponding component is another principal issue for practical applications. Radiography includes several steps. Loading the film into the protective envelope and then into the insert channel takes around 1 min, exposure times and discharging were typically  $\sim 5$  min, handling and development of the film add another 10 min. The average, very fast manual analysis of the film takes around 4 minutes. Automatic scanning of the film would add several hours. It is recommended especially because of easier image manipulation and analysis. Thus, the minimum time necessary for one radiographic measurement is up to 20 minutes and it would be considerably longer if film scanning were included. Because of narrow dynamic range and insert wall changes, at least three different exposures are required for the full inspection of the insert wall. Thus, 20 cm of the channel length can be inspected within approximately 1 hour. Obviously, the time necessary for the radiography of all 8 channels in 5 m long canister is too long for large-scale industrial production. Faster radiographic methods, e.g. digital radiography or radioscopy, are required for industrial NDE.

## 5. Conclusions

Radiography combined with subsequent metallographic investigations of the microstructure of ductile cast iron insert for geological disposal of spent nuclear fuel, which were performed on the as-produced and deformed inserts, revealed:

- variety of microstructure defects, including small variations in carbon nodule size, density and shape, blowholes and pinholes, sand-like inclusions and their agglomerates, oxide-filled cracks as well as debonding and surface defects at the interface with steel tubes. Additional cracks were observed in the outer walls of the deformed mock-up;

- large sand inclusions mainly concentrated at the inner surfaces of the insert walls. They seem to originate from insufficient cleaning of the steel tubes prior to casting;

- the largest microstructure defects located in the zone of local tensile stresses – slag inclusions and their agglomerates and large oxide-filled cracks around them – are deemed to be critical for crack initiation and growth. They can reach size of several millimeters whereas all the other defects are maximum several hundred microns in size. Large blowholes, which were occasionally present in the inner walls around the bridges fixing position of steel tubes, were out of the regions of stress concentration;

- the resolutions of D2 and D4 films of 1.25 mm and 2.5 mm deep cracks, respectively, are sufficient to detect critical defects in the studied DCI inserts;

- film radiography is suitable for the detection of

such defects as blowholes, debonding, slag inclusions and their agglomerates, and cracks, which are oriented parallel to the beam;

- despite high resolution, conventional film radiography is too time-consuming for industrial inspection of real size DCI inserts. Faster digital radiography or radioscopy techniques have to be considered for large scale NDE of spent nuclear fuel canisters.

## Acknowledgements

The contribution and help of M. Prieto with metallography and E. Conceição with SEM observations are gratefully acknowledged.

## References

- [1] Towards a European Strategy for the Security of Energy Supply. Final Report on the Green Paper on Energy, Energy and Transport DG, EC, Bruxelles 2005. ISBN 92-894-8419. Available at [http://europa.eu.int/comm/energy\\_transport/en/lpi\\_lv\\_en1.html](http://europa.eu.int/comm/energy_transport/en/lpi_lv_en1.html)
- [2] Programme for research, development and demonstration of methods for treatment and final disposal of nuclear waste, including social impact research. Swedish Nuclear Waste Management. FuD – program 2004. Available at [www.skb.se](http://www.skb.se)
- [3] ANDERSSON, C.-G.—ANDERSSON, M.—ERIXON, B.—BJÖRKGREN, L.-E.—DILLSTRÖM, P.—MINNEBO, P.—NILSSON, K.-F.—NILSSON, F.: Probabilistic analysis and material characterization of canister insert for spent nuclear fuel. Summary report, Technical Report TR-05-17, Svensk Kärnbränslehantering AB, Sweden 2005. Available at [www.skb.se](http://www.skb.se)
- [4] ANDERSSON, C.-G.—ERIKSSON, P.—WESTMAN, M.—EMILSSON, G.: Status report, canister fabrication, TR-04-23, Svensk Kärnbränslehantering AB, Sweden 2004. Available at [www.skb.se](http://www.skb.se)
- [5] NILSSON, K.-F.—BLAGOEVA, D.—MORETTO, P.: Eng. Fracture Mechanics, 73, 2006, p. 1133.
- [6] NILSSON, K. F.—MINNEBO, P.—BLAGOEVA, D.: J. Mat. Eng. Performance, 2006 (in press).
- [7] LOFAJ, F.—METTEN, L.—VAN DE SANDE, A.—SELDIS, T.—NILSSON, K.-F.—ERIKSSON, A.: Ultrasonic and Radiography Investigations of Defects in Ductile Cast Iron Casks for Disposal of Spent Nuclear Fuel. Eureport EUR 22145 EN, DG JRC – Institute for Energy, Petten, The Netherlands 2005.
- [8] DILLSTRÖM, P.: Probabilistic analysis of canister inserts for spent nuclear fuel. Technical report SKB TR-05-19, Svensk Kärnbränslehantering AB, Sweden 2005. Available at [www.skb.se](http://www.skb.se)
- [9] NEN-EN 1563:1997, European standard, Founding-Spheroidal graphite, CEN, 1997.
- [10] NILSSON, K.-F.—LOFAJ, F.—BURSTRÖM, M.—ANDERSSON, C.-G.: Pressure tests of two KBS-3 canister mock-ups. Technical report TR-05-18, Svensk Kärnbränslehantering AB, Sweden 2005. Available at [www.skb.se](http://www.skb.se)
- [11] NILSSON, K.-F.—BURSTRÖM, M.—LOFAJ, F.—ANDERSSON, C.-G.: Eng. Failure Analysis, 14, 2007, p. 47.